

Temperature-Dependent Ultrasonic Properties of Semiconducting M_2CO_2 (M= Ti, Zr, Hf) MXenes

P. K. Yadawa^{1*}, N. Chaurasiya^{1,2}, S. Rai¹, A. K. Prajapati¹

¹Department of Physics, Prof. Rajendra Singh (Rajju Bhaiya) Institute of Physical Sciences for Study and Research, V. B. S. Purvanchal University, Jaunpur, India- 222003

²Department of Mechanical Engineering, UNSIET, V. B. S. Purvanchal University, Jaunpur, India- 222003

Received 12 December 2021, accepted in final revised form 20 May 2022

Abstract

Here, we have studied the elastic, ultrasonic, mechanical, and thermal behavior of temperature-dependent hexagonal oxygen-functionalized M_2CO_2 (M= Ti, Zr, Hf) MXenes. The higher-order linear and nonlinear elastic constants, viz., second-order (SOECs), and third-order (TOECs) have been computed using the Lenard Jones interaction potential model. For mechanical characterization, bulk modulus (B), shear modulus (G), Young's modulus (Y), Pugh's ratio (B / G), Poisson's ratio, and anisotropic index are evaluated using SOECs. Born's stability and Pugh's criteria are used to examine the nature and strength of the MXenes in all the temperatures. For the investigation of anisotropic behavior and its thermophysical properties, temperature-dependent ultrasonic velocities and thermal relaxation time have been calculated along with different orientations from the unique axis of the crystal. The ultrasonic attenuation (UA) of a longitudinal and shear wave due to phonon-phonon (p-p) interaction and thermoelastic relaxation mechanism were investigated for these oxygen-functionalized MXenes. Thermal conductivity is a principal contributor to the behavior of UA due to p-p interactions. Our analysis suggests that semiconductor Ti_2CO_2 MXenes show superior mechanical properties to other oxygen-functionalized MXenes. Computed elastic, ultrasonic, and thermal properties are correlated to evaluate the microstructural behavior of the materials useful for industrial applications.

Keywords: Oxygen-functionalized semiconducting MXenes; Mechanical properties; Thermal conductivity; Elastic properties; Ultrasonic properties.

© 2022 JSR Publications. ISSN: 2070-0237 (Print); 2070-0245 (Online). All rights reserved.
doi: <http://dx.doi.org/10.3329/jsr.v14i3.56976> J. Sci. Res. **14** (3), 735-748 (2022)

1. Introduction

Two-dimensional (2D) compounds have attracted attention in condensed material physics due to their excellent properties and potential applications [1,2]. 2D compounds have many different thermal and electronic properties than their bulk counterparts [3]. In the past two decades, the size has continuously decreased during the growth of highly integrated electronic components of electronic devices. The determinations of the

*Corresponding author: pk Yadawa@gmail.com

performance of electronic devices, a moderate electronic bandgap, efficient heat dissipation, and high carrier mobility have become correspondingly important characteristics [4]. Graphene (2D material) [5] has been established to keep a charge carrier mobility and high thermal conductivity [6], which has strongly stimulated continuing investigation into growing its applicability as a material for electronic devices. Thus, developing a required 2D semiconducting compound with an acceptable intrinsic thermal conductivity, sensible bandgap, and higher carrier mobility has the main goal of research in materials science.

MXenes have become promising materials for several mechanical and engineering applications due to their outstanding physicochemical advantages, excellent strength, multilayered structures, and good electrical conductivity [7]. The general formulation of MXene is $M_{n+1}X_nT_x$ ($n = 1-4$). Here 'M' signifies transition metals, 'A' represents an A-group element in the Periodic Table, 'X' is carbon/nitrogen, and T_x represents surface functional groups (OH, O, Cl, F) [8].

The mechanical, structural, and electronic properties of M_2CT_2 ($M=Sc, Ti, V, Cr, Zr, Nb, Mo, Hf, Ta, W$) MXenes have shown that the surface functional groups ($T = F, OH, O$) and transition metal atom [9]. The oxygen functionalized MXene structures have shown superior mechanical stability compared to hydroxyl and fluorine functionalized compounds. Also, MXene structures have been reported by several other researchers for their structural, electronic, and thermal properties. The thermal and electronic properties of Sc_2CT_2 ($T=F, OH$) have been investigated by Zha *et al.* [10-12], Hf_2CO_2 , Ti_2CO_2 [13], and Zr_2CO_2 [14] MXene compounds. Moreover, Gandi *et al.* [15] have evaluated the TE properties of M_2CO_2 ($M=Ti, Zr, Hf$) MXene structures and found the bandgap increases with increasing the mass of the transition metal. Also, Yorulmaz *et al.* [16] have studied the mechanical and dynamical stability of M_2XT_2 ($M=Sc, Mo, Ti, Zr, Hf; X=C, N; T=O, F$) MXene structures. The MXene Ti_2CO_2 has presented a semiconducting characteristic with higher carrier mobility [17] and higher thermodynamic stability [18]. Ti_2CO_2 MXene has deserved more comprehensive investigations due to its excellent properties and potential applications [19].

Recent investigations have suggested considerable interest in MXenes due to their vast potential for use in electronic devices etc. Given the aforementioned potential applications, the complete knowledge of the mechanical and physical properties of these MXenes, however, is still lacking. For example, the nonlinear elastic mechanical properties, such as all higher order elastic constants, attenuation, etc., have not been addressed yet; therefore, in the present work, we predict the ultrasonic properties of these MXenes.

Ultrasonic properties are significant for studying the physical characteristics of the materials, such as thermal relaxation time, energy density, and thermal conductivity. Ultrasonic attenuation (UA) is the exact main physical parameter to describe nanocrystalline materials, whichever appreciates the specific relationship between the anisotropic behavior of proximal hematitic planes and some physical measures like

thermal energy density, specific heat, and thermal conductivity, which are well associated with higher-order elastic constants [20].

In the present work, we have investigated the ultrasonic, elastic, and thermal properties of oxygen-functionalized semiconducting M_2CO_2 ($M= Ti, Zr, Hf$) MXenes. Microstructural properties are correlated with thermophysical properties, and the mechanical behavior of these semiconducting MXenes has been analyzed comprehensively. We have evaluated higher-order elastic constants, acoustic coupling constants, ultrasonic attenuation coefficient, elastic stiffness constant, thermal relaxation time, and the ultrasonic velocities of these oxygen-functionalized MXenes. The shear modulus (G), bulk modulus (B), Young's modulus (Y), Poisson's ratio, Pugh's ratio (B / G), and anisotropic parameters were also calculated and discussed for these semiconducting MXenes.

2. Theory

The technique based on the interaction potential model is one of the well-established methods for calculating second and third-order elastic constants (SOECs and TOECs) of hexagonally structured material. In this work, the Lenard Jones interaction potential model approach was used to evaluate SOECs. The higher-order elastic constants can be calculated by estimating elastic energy density with strain. Taking the approximation of the interaction potential up to the second nearest neighbors, the crystal symmetry exhibits the six second-order elastic constants (SOECs) and ten third-order elastic constants (TOECs), given as follows [21-23].

$$\left. \begin{aligned}
 C_{11} &= 24.1 p^4 C' & G_{12} &= 5.918 p^4 C' \\
 C_{13} &= 1.925 p^6 C' & C_{33} &= 3.464 p^8 C' \\
 C_{44} &= 2.309 p^4 C' & C_{66} &= 9.851 p^4 C' \\
 C_{111} &= 126.9 p^2 B + 8.853 p^4 C' & C_{112} &= 19.168 p^2 B - 1.61 p^4 C' \\
 C_{113} &= 1.924 p^4 B + 1.155 p^6 C' & G_{123} &= 1.617 p^4 B - 1.155 p^6 C' \\
 C_{133} &= 3.695 p^6 B & C_{155} &= 1.539 p^4 B \\
 C_{144} &= 2.309 p^4 B & C_{344} &= 3.464 p^6 B \\
 C_{222} &= 101.039 p^2 B + 9.007 p^4 C' & C_{333} &= 5.196 p^6 B
 \end{aligned} \right\} \tag{1}$$

where, $p = c/a$ represents axial ratio; $C' = \chi a / p^5$; $B = \psi a^3 / p^3$. χ and ψ denote the harmonic and anharmonic parameters, respectively, and are given as:

$$\chi = (1/8)[\{nb_0(n-m)\} / \{a^{n+4}\}] \tag{2}$$

$$\psi = -\chi / \{6a^2(m+n+6)\} \tag{3}$$

Where, m and n are positive integers, and b_0 is the constant.

Bulk modulus (B) and shear modulus (G) were calculated using Voigt and Reuss' methodologies [24-26]. Using Hill's approach, average modulus values obtained from both methods are taken for more accurate results [27, 28]. Young's modulus (Y) and

Poisson's ratio (σ) are calculated using values of B and G [29,30]. The following expressions were used for this evaluation:

$$\left. \begin{aligned} M &= C_{11} + C_{12} + 2C_{33} - 4C_{13}; & C^2 &= (C_{11} + C_{12})C_{33} - 4C_{13} + C^2_{13}; \\ B_R &= \frac{C^2}{M}; & B_V &= \frac{2(C_{11}+C_{12})+4C_{13}+C_{33}}{9}; \\ G_V &= \frac{M+12(C_{44}+C_{66})}{30}; & G_R &= \frac{5C^2C_{44}C_{66}}{2[3B_V C_{44}C_{66}+C^2(C_{44}+C_{66})]}; \\ Y &= \frac{9GB}{G+3B}; & B &= \frac{B_V+B_R}{2}; & G &= \frac{G_V+G_R}{2}; & \sigma &= \frac{3B-2G}{2(3B+G)} \end{aligned} \right\} \quad (4)$$

The mechanical and anisotropic properties of materials are studied by estimating the ultrasonic velocity. There are three types of propagation modes of the ultrasonic wave in the hexagonal structured materials. One of them is a longitudinal mode (V_L), and the other two are shear modes (V_{S1} , V_{S2}). The terms for ultrasonic velocities and Debye average velocity are given in our earlier research works [31,32].

For hexagonal structured crystal, the Debye average is given by [31]:

$$V_D = \left[\frac{1}{3} \left(\frac{1}{V_L^3} + \frac{1}{V_{S1}^3} + \frac{1}{V_{S2}^3} \right) \right]^{-1/3} \quad (5)$$

When the ultrasonic waves propagate through the material, the equilibrium of lattice phonon distribution gets disturbed. The time takes for the re-establishment of equilibrium of the thermal phonons is named thermal relaxation time, denoted by τ , and is given by the following expression [32]:

$$\tau = \tau_S = \tau_L/2 = \frac{3k}{c_V V_D^2} \quad (6)$$

where the thermal relaxation time for the longitudinal wave and shear wave is represented by τ_L and τ_S respectively, k is the thermal conductivity of the material.

The mathematical formulation of ultrasonic attenuation for longitudinal (α_{Long}) and shear waves (α_{Shear}) induced by the energy loss due to electron-phonon interaction is given by [21,31,32]:

$$\alpha_{long} = \frac{2\pi^2 f^2}{\rho V_l^3} \left(\frac{4}{3} \eta_e + \chi \right) \quad (7)$$

$$\alpha_{shear} = \frac{2\pi^2 f^2}{\rho V_s^3} \eta_e \quad (8)$$

where ' ρ ' is the density of nanostructured compound, ' η_e ' is the electron viscosity, ' f ' is the frequency of the ultrasonic wave, and ' χ ' is the compressional viscosity, V_L and V_S are the acoustic wave velocities for longitudinal and shear waves respectively.

P-p interaction (Akhieser's type loss) (at high temperature) and thermoelastic loss are the two prevailing processes, whichever are considerable for attenuation of ultrasonic waves. The subsequent equation specifies the attenuation by Akhieser's loss:

$$(\alpha/f^2)_{Akh} = \frac{4\pi^2 \tau E_0 (D/3)}{2\rho V^3} \quad (9)$$

Here, f represents the frequency of the ultrasonic wave; E_0 is the thermal energy density. The measure of transforming acoustic energy into thermal energy is known as acoustical coupling constants (D) is given by Eq. 10:

$$D = 3(3E_0 \langle \gamma_i^j \rangle^2 - \langle \gamma_i^j \rangle^2 C_V T) / E_0 \tag{10}$$

where C_V is the specific heat per unit volume of the material, T is the temperature and γ_i^j is the Grüneisen number.

The thermoelastic loss $(\alpha/f^2)_{Th}$ is evaluated by the following equation [21,22]:

$$(\alpha/f^2)_{Th} = 4\pi^2 \langle \gamma_i^j \rangle^2 \frac{kT}{2\rho v_L^5} \tag{11}$$

3. Results and Discussion

3.1. Higher-order elastic constants

We have calculated the elastic constants (six SOECs and ten TOECs) in the current analysis using Lennard-Jones's potential model. The lattice parameters ‘a’ (basal plane parameter) and ‘p’ (axial ratio) for Ti_2CO_2 , Zr_2CO_2 , Hf_2CO_2 are 3.036Å, 3.310Å, 3.266 Å and 2.267, 1.870, 1.846 respectively [33]. The value of parameter 'b₀' taken under equilibrium conditions for minimum energy of the nanocrystalline structure is 2.64×10^{-64} erg cm⁷, 6.18×10^{-64} erg cm⁷, 5.92×10^{-64} erg cm⁷ for Ti_2CO_2 , Zr_2CO_2 , Hf_2CO_2 respectively. The values of m and n are considered 6 and 7, respectively, for all the semiconducting MXenes. SOECs and TOECs were calculated for these M_2CO_2 (M= Ti, Zr, Hf) MXenes are shown in Table 1.

Table 1. Second and third-order elastic constants (SOECs and TOECs) in (GPa) at room temperature.

Compound	C ₁₁	C ₁₂	C ₁₃	C ₃₃	C ₄₄	C ₆₆	[33] C ₁₁
Ti ₂ CO ₂	369	91	152	1401	182	144	368
Zr ₂ CO ₂	441	108	123	776	147	173	440
Hf ₂ CO ₂	490	120	133	817	160	192	490

Compound	C ₁₁₁	C ₁₁₂	C ₁₁₃	C ₁₂₃	C ₁₃₃	C ₃₄₄	C ₁₄₄	C ₁₅₅	C ₂₂₂	C ₃₃₃
Ti ₂ CO ₂	-7190	-	-316	-401	-2620	-2450	-460	-	-5700	-1290
Zr ₂ CO ₂	-7950	1140	-341	-434	-2760	-2580	-506	312	-6310	-1320
Hf ₂ CO ₂	-6020	-	-388	-493	-4730	-4430	-575	-	-4760	-3420
		1260						337		
		-954						-		
								383		

M_2CO_2 (M= Ti, Zr, Hf) MXenes had the highest elastic constant, which is important for the material associated with the stiffness parameter. SOECs are used to determine the ultrasonic attenuation and allied parameters. The higher values of elastic constant for MXenes show their better mechanical properties.

Evidently, for steady of the nanostructured MXenes, the five independent SOECs (C_{ij}, namely C₁₁, C₁₂, C₁₃, C₃₃, C₄₄) would satisfy the well-known Born- Huang’s stability

norms [26,27] i.e. $C_{11} - |C_{12}| > 0$, $(C_{11}+C_{12}) C_{33} - 2C_{13}^2 > 0$, $C_{11} > 0$ and $C_{44} > 0$. From Table-1, it is obvious that the values of elastic constant are positive, too satisfying Born-Huang's mechanical stability constraints, and therefore semiconducting MXenes are mechanically stable. The evaluated values of second-order elastic constant C_{11} of Ti_2CO_2 , Zr_2CO_2 , Hf_2CO_2 are 369 GPa, 441 GPa, and 490 GPa, respectively [Table 1], which values are the same as evaluated by Zha *et al.* [33]. Thus, there is good agreement between the presented and the reported values of elastic constants. Therefore, our theoretical methodology is well justified for evaluating SOECs of these semiconducting M_2CO_2 (M= Ti, Zr, Hf) MXenes. The calculated values of TOECs are also presented in Table 1. Its negative values of third-order elastic constants indicate a negative strain in the solid. The negative TOECs appear in the previous papers on hexagonal structure material. Therefore, the theory applied to evaluate higher-order elastic constants is justified [21,23,32]. Hence, the applied theory for the valuation of higher-order elastic constants is well justified.

The mechanical properties of the materials can be examined using the linear elastic constants (SOECs). Here, we have used the values of SOECs for the determination of Young's modulus (Y), bulk modulus (B), shear modulus (G), and Poisson's ratio (σ) using the Voigt-Reuss-Hill averaging scheme and presented in Table 2.

Table 2. Voigt–Reuss' constants (M and C^2), Bulk modulus in (GPa), Shear Modulus in (GPa), Young's Modulus in (GPa), Poisson's Ratio, Pugh's Ratio, for semiconducting M_2CO_2 (M= Ti, Zr, Hf) MXenes.

Compound	M	C^2	B_r	B_v	G_r	G_v	Y	B/G	G/B	σ
Ti_2CO_2	2655	6057	138	325	355	218	83	2.43	0.04	0.48
Zr_2CO_2	1608	3918	243	262	342	181	58	1.03	0.96	0.11
Hf_2CO_2	1712	4630	270	285	175	185	44	1.54	0.64	0.23

These mechanical constants play a crucial role in determining the strength of the crystals. As per Pugh's criterion, the ratio of shear modulus to bulk modulus, G/B, is used to specify the brittle/ ductile nature of the materials. A lower G/B value (< 0.5) indicates ductility, whereas a higher value (> 0.5) shows the brittle behavior of the material [24,25]. These semiconducting MXenes have little Stiffness. B/G and ' σ ' are the measures of brittleness and ductility of solid. If $\sigma \leq 0.26$ and $B/G \leq 1.75$, the solid is generally brittle; otherwise, it is ductile in nature [24, 25]. Our finding of lower B/G and σ compared to their critical values indicates that Zr_2CO_2 and Hf_2CO_2 MXenes are brittle in nature, while Ti_2CO_2 is ductile in nature [Table 2]. It is well known that for the stability of the material, the value of σ should be less than 0.5. The values of ' σ ' evaluated for semiconducting M_2CO_2 (M= Ti, Zr, Hf) MXenes are smaller than their critical value. It indicates that these MXenes are stable against shear. The compressibility, hardness, ductility, toughness, brittleness, and bonding characteristic of the nanostructured material are too well connected with the second-order elastic constants.

Elastic anisotropic is an essential parameter for mechanical properties of the materials. The elastic anisotropic is defined by the following formulations for hexagonally structured materials [34]:

$$\Delta P = C_{33} / C_{11},$$

where ΔP is the anisotropy for compressional waves.

$$\Delta_{S1} = (C_{11} + C_{33} - 2C_{13}) / 4C_{44}$$

$$\Delta_{S2} = 2C_{44} / (C_{11} - C_{12})$$

where Δ_{S1} and Δ_{S2} are the anisotropy for the shear waves, polarized perpendicular to the basal plane and polarized in the basal plane respectively.

The computed compressional anisotropy of semiconducting M_2CO_2 (M= Ti, Zr, Hf) MXenes is $\Delta P = 3.80, 1.76, 1.67$, respectively. These semiconducting materials are further easily compressed in the [001] direction than [100] direction. The value of shear anisotropy Δ_{S1} and Δ_{S2} are 2.01, 1.65, 1.63, and 1.31, 0.88, and 0.86, respectively. The compressional anisotropy is large due to the large values of C_{33} . It shows that the major shear distortion occurs in [100] plane and the error is most likely to occur between planes parallel to the [001] plane. In isotropic medium, $\Delta P = \Delta_{S1} = \Delta_{S2} = 1$. Thus, these semiconducting materials are anisotropic. These results designate that the M_2CO_2 (M= Ti, Zr, Hf) MXenes are stronger in the layer which is parallel to the [001] plane than between the layers.

3.2. Ultrasonic velocity and allied constraints

The ultrasonic velocity is useful for studying the mechanical and isotropic characteristics of the material, and it is well associated with the SOECs and density of the materials. Here, we have calculated the longitudinal ultrasonic velocity (V_L), two ultrasonic shear velocities (V_{S1}, V_{S2}), and the Debye average velocity (V_D). The temperature-dependent density (ρ) values of these semiconducting MXenes are presented in Table 3 and have been taken from the literature [23]. Also, the temperature-dependent thermal conductivity of these MXenes has been taken from Zha *et al.* [33]. The values of temperature-dependent thermal energy density (E_0) and specific heat per unit volume (C_V) were calculated using the Tables of physical constant. The temperature-dependent specific heat per unit volume, thermal energy density, thermal conductivity, and acoustic coupling constants (D_L and D_S) are presented in Tables 3-5.

Table 3. Density (ρ : in 10^3 kg m^{-3}), specific heat per unit volume (C_V : in $10^5 \text{ Jm}^{-3}\text{K}^{-1}$), thermal energy density (E_0 : in 10^8 Jm^{-3}), thermal conductivity (k : in $\text{Wm}^{-1}\text{K}^{-1}$), and acoustic coupling constant (D_L, D_S) of semiconducting Ti_2CO_2 MXene.

Temp	ρ	C_V	E_0	k	D_L	D_S
200	8.47	9.34	0.77	30.00	23.13	17.12
400	8.43	13.22	3.11	16.25	23.11	18.23
600	8.34	14.14	5.85	13.75	23.10	18.28

Table 4. Density (ρ : in 10^3 kg m^{-3}), specific heat per unit volume (C_V : in $10^5 \text{ Jm}^{-3}\text{K}^{-1}$), thermal energy density (E_0 : in 10^8 Jm^{-3}), thermal conductivity (k : in $\text{Wm}^{-1}\text{K}^{-1}$), and acoustic coupling constant (D_L , D_S) of semiconducting Zr_2CO_2 MXene.

Temp	ρ	C_V	E_0	k	D_L	D_S
200	12.82	10.93	1.09	87.50	35.88	13.34
400	12.78	13.25	3.55	47.50	36.49	12.12
600	12.74	13.66	6.23	33.75	36.67	12.11

It is clear from Tables 3-5 that the values of D_L are larger than D_S for M_2CO_2 (M= Ti, Zr, Hf) MXenes. It indicates that the transformation of ultrasonic energy into thermal energy for the longitudinal ultrasonic wave is greater than for the shear ultrasonic waves.

Table 5. Density (ρ : in 10^3 kg m^{-3}), specific heat per unit volume (C_V : in $10^5 \text{ Jm}^{-3}\text{K}^{-1}$), thermal energy density (E_0 : in 10^8 Jm^{-3}), thermal conductivity (k : in $\text{Wm}^{-1}\text{K}^{-1}$), and acoustic coupling constant (D_L , D_S) of semiconducting Hf_2CO_2 MXene.

Temp	ρ	C_V	E_0	k	D_L	D_S
200	23.93	12.75	1.42	120.0	35.97	12.12
400	23.89	14.31	4.18	67.5	35.52	13.34
600	23.85	14.61	7.07	47.5	35.65	13.34

The angular dependences of ultrasonic wave velocity (V_L , V_{S1} , V_{S2} , and V_D) at different temperatures are presented in Fig. 1. The angles are taken from the z-axis of the crystal. From Fig. 1a-c, it is clear that V_L has decreased with temperatures, while V_{S1} has a maximum of 55° along the z-axis of the crystal. Also, V_{S2} is approximately unchanged with the angle from the z-axis. Further, orientation-dependent ultrasonic behavior is anomalous due to the combined effect of second-order elastic constants and density. Similar nature of the angle-dependent ultrasonic velocity is also reported for other hexagonal structured materials [35,36]. The Debye average velocity (V_D) variation with the angle is displayed in Fig. 1d. As orientation changes, the V_D increases with angle, and at a critical angle, $\theta = 55^\circ$, it becomes maximum; after this, it decreases. Thus, this critical angle is the best direction for propagating the ultrasonic wave in the M_2CO_2 (M= Ti, Zr, Hf) compounds. These orientation-dependent characteristics of the Debye average velocity, along with its constituents' modes (V_L , V_{S1} , and V_{S2}) will be useful for the determination of anisotropic properties of the hexagonally structured materials [31,32].

When an ultrasonic wave passes through the medium, it disturbs the equilibrium phonons. These phonons return to their equilibrium state after a certain time, called thermal relaxation time ' τ ' [35]. The orientation-dependent thermal relaxation time curves are reciprocal nature of V_D as $\tau \propto 3k/C_V V_D^2$. It is clear that the thermal relaxation time for M_2CO_2 (M= Ti, Zr, Hf) MXenes are mainly affected by the thermal conductivity. The thermal relaxation time ' τ ' is the order of picoseconds for these semiconducting MXenes (Fig. 2) [39-42]. Therefore, the evaluated thermal relaxation time explains the semiconducting M_2CO_2 (M= Ti, Zr, Hf) compounds. The minimum value of ' τ ' for wave propagation along $\theta = 45^\circ$ denotes that the re-establishment time for equilibrium distribution of thermal phonons will be minimum for wave propagation along this

direction. This shows that the distribution of thermal phonons restores its equilibrium in this period after passing the sound wave. The information on thermal relaxation time and ultrasonic velocity will play a crucial role in determining ultrasonic absorption in the medium.

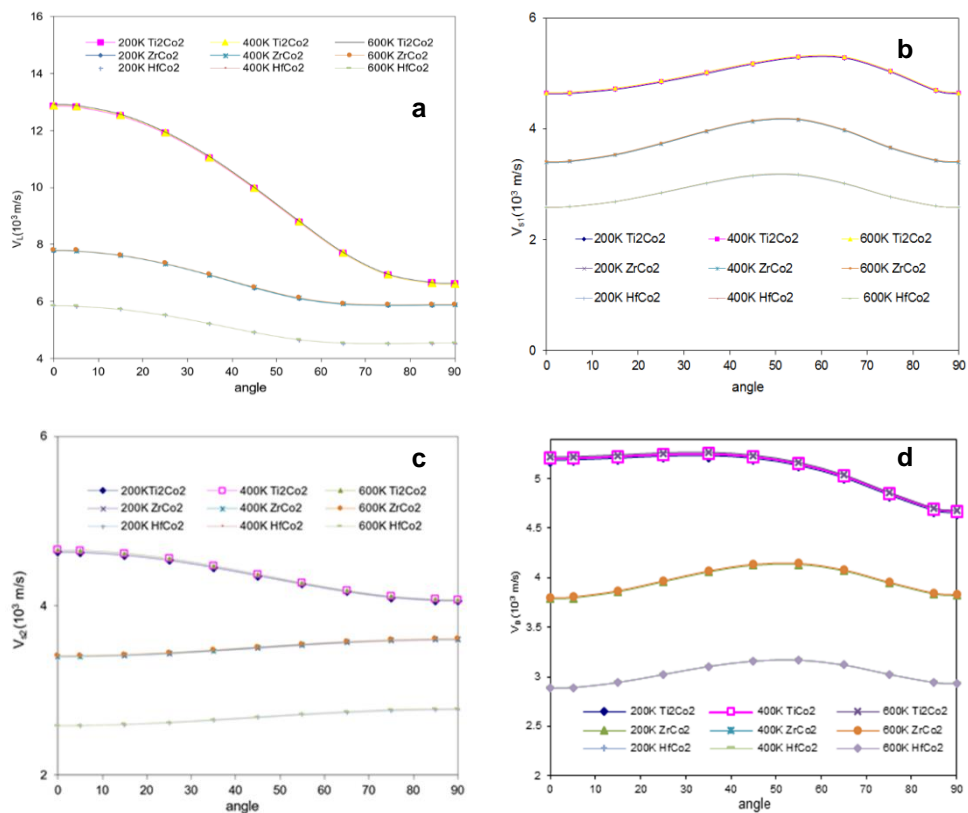


Fig. 1. (a) V_L vs. angle with the z-axis of crystal; (b) V_{S1} vs. angle with the z-axis of crystal; (c) V_{S2} vs. angle with the z-axis of crystal; (d) V_D vs. angle with the z-axis of crystal.

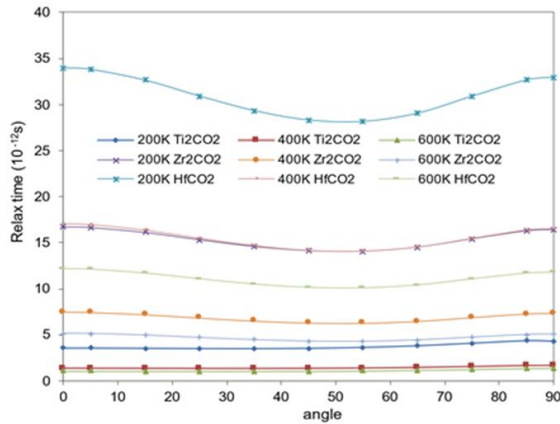


Fig. 2. Relaxation time vs. angle with the z-axis of crystal.

3.3. Ultrasonic attenuation due to p-p interaction and thermal relaxation occurrences

While evaluating ultrasonic attenuation, the wave is propagating along the z-axis [$\langle 001 \rangle$ direction] of M_2CO_2 ($M = Ti, Zr, Hf$) MXenes. The ultrasonic attenuation coefficient divided by frequency squared $(\alpha/f^2)_{Akh}$ is calculated for the longitudinal wave $(\alpha/f^2)_L$ and the shear wave $(\alpha/f^2)_S$ using Eqn. 9 under the condition $\omega\tau \ll 1$ at different temperatures. Eqn. 11 has been used to calculate the thermo-elastic loss divided by frequency squared $(\alpha/f^2)_{Th}$. Fig. 3 present the values of the temperature-dependent $(\alpha/f^2)_L$, $(\alpha/f^2)_S$, $(\alpha/f^2)_{Th}$ of M_2CO_2 ($M = Ti, Zr, Hf$) MXenes.

In the present work, the ultrasonic wave is propagated along the z-axis of the crystal [Fig. 3a,b], it is clear that the Akhieser type of energy losses for the longitudinal waves, shear waves, and the thermo-electric loss increase with the temperature of compounds. $(\alpha/f^2)_{Akh}$ is proportional to $D, E_0, \tau,$ and V^{-3} . Tables 3-5 show that E_0 and V increase with temperature. Hence, Akhieser losses in semiconducting M_2CO_2 ($M = Ti, Zr, Hf$) MXenes are overwhelmingly affected by E_0 and the k' . Therefore, the increase in UA is due to decreased thermal conductivity. Thus, ultrasonic attenuation is mainly governed by the phonon-phonon interaction mechanism. A comparison of the ultrasonic attenuation could not be made due to the lack of experimental data in the literature.

From Fig. 3c, it is clear that the thermo-elastic losses are much smaller than Akhieser loss for semiconducting M_2CO_2 ($M = Ti, Zr, Hf$) MXenes, Ultrasonic attenuation due to p-p interaction for longitudinal wave and the shear wave is a leading factor. The thermal conductivity and thermal energy density are the main factors that affect the total attenuation. Thus, it may be predicted that these MXenes behave in their purest form at low temperature and further ductile nature by the minimum attenuation. At higher temperatures, these semiconducting MXenes are the least ductile. Therefore, at low temperature (200K) there will be the least impurity in all chosen MXenes. The minimum UA for M_2CO_2 ($M = Ti, Zr, Hf$) MXenes minimum defends its quite stable state. Also,

mechanical things of these semiconductor MXenes crystals are superior at low temperatures because they have the least ultrasonic attenuation and defend their rather stable hexagonal type structure state.

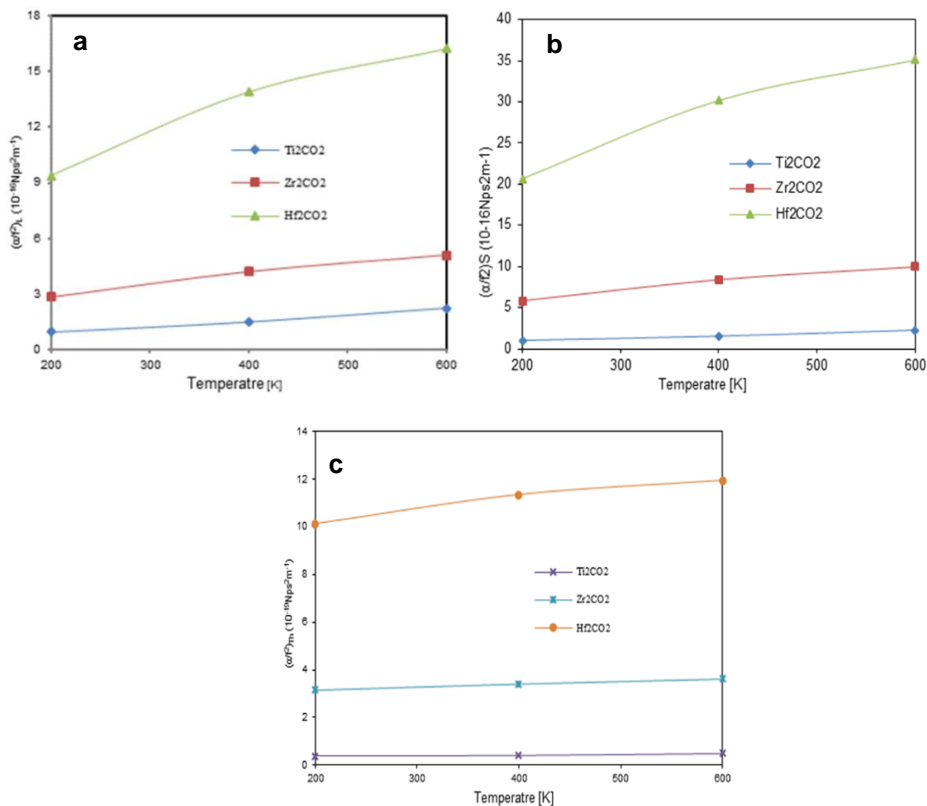


Fig. 3. (a) $(\alpha / f^2)_L$ vs temperature of M_2CO_2 MXenes; (b) $(\alpha / f^2)_S$ vs temperature of M_2CO_2 MXenes, (c) $(\alpha / f^2)_{Th}$ vs. temperature of M_2CO_2 (M= Ti, Zr, Hf) MXenes.

4. Conclusion

We have computed higher order elastic constants for temperature-dependent oxygen-functionalized semiconducting M_2CO_2 (M= Ti, Zr, Hf) MXenes using the Lenard Jones interaction potential approaches. The theoretical methodology is justified for evaluating SOECs and TOECs of MXenes. It has been found that the M_2CO_2 (M= Ti, Zr, Hf) MXenes are mechanically stable. The M_2CO_2 (M= Ti, Zr, Hf) MXenes have anisotropic structures, which designate that these MXenes are stronger in the layer that one is parallel to the [001] plane than in other layers. Acoustic coupling constants of these MXenes show that the transformation of ultrasonic energy into thermal energy is greater than the shear ultrasonic waves. The thermal relaxation time is found to be of the order of picoseconds, which shows their hexagonal structure. As ' τ ' has the smallest value along $\theta = 45^\circ$ at all

temperatures, the time for re-establishment of the equilibrium distribution of phonons will be minimum for the wave propagation in this direction. The ultrasonic attenuation due to the phonon-phonon interaction mechanism is predominant over total attenuation as a governing factor of thermal conductivity. The mechanical properties of the semiconducting Ti₂CO₂ MXene are better than other M₂CO₂ (M=Zr, Hf) MXenes at low temperatures (50 K). Thus, semiconducting Ti₂CO₂ MXenes behave in their purest form and are further ductile, demonstrated by the minimum attenuation, while other MXenes are the least ductile. These semiconducting M₂CO₂ (M= Ti, Zr, Hf) MXenes have minimum attenuation at low temperatures.

Acknowledgments

Authors are thankful to Veer Bahadur Singh Purvanchal University (133/VBSPU/IQAC/2022, Date. 23-03-2022) minor project grant (Code:50) and Council for Scientific and Industrial Research – University Grant Commission (CSIR – UGC) for providing financial assistance in form of CSIR - Junior Research Fellowship (1500/CSIR-UGC NET Dec, 2017) India.

References

1. C. Lee, X. Wei, J.W. Kysar, and J. Hone, *Science* **321**, 385 (2008).
<https://doi.org/10.3390/ma13081980>
2. A. A. Balandin, S. Ghosh, W.Z. Bao, I. Calizo, D. Teweldebrhan, F. Miao, and C.N. Lau, *Nano Lett.* **8**, 902 (2008). <https://doi.org/10.1021/nl0731872>
3. L. Yu, Y.-H. Lee, X. Ling, E. J. G. Santos, Y. Ch. Shin, Y. Lin, M. Dubey, E. Kaxiras, J. Kong, H. Wang, and T. Palacios, *Nano Lett.* **14**, 3055 (2014).
<https://doi.org/10.1021/nl404795z>
4. J. Qiao, X. Kong, Z.-X. Hu, F. Yang, and W. Ji, *Nat. Commun.* **5**, 4475 (2014).
<https://doi.org/10.1038/ncomms5475>
5. K. S. Novoselov, A. K. Geim, S. V. Morozov, D. Jiang, Y. Zhang, S. V. Dubonos, V. Grigorieva, and A. A. Firsov, *Science* **306**, 666 (2004).
<https://doi.org/10.1126/science.1102896>
6. A. A. Balandin, S. Ghosh, W. Bao, I. Calizo, D. Teweldebrhan, F. Miao, and C. Ning Lau. *Nano Lett.* **8**, 902 (2008). <https://doi.org/10.1021/nl0731872>
7. Y. Ibrahim, A. Mohamed, A. M. Abdelgawad, K. Eid, A. M. Abdullah, and A. Elzatahry, *Nanomaterials* **10**, 1916 (2020). <https://doi.org/10.3390/nano10101916>
8. G. Deysheer, C. E. Shuck, K. Hantanasirisakul, N. C. Frey, A. C. Foucher, K. Maleski, A. Sarycheva, V. B. Shenoy, E. A. Stach, and B. Anasori, *ACS Nano* **14**, 204 (2020).
<https://doi.org/10.1021/acsnano.9b07708>
9. A. Champagne and J. -C. Charlier, *J. Phys. Mater.* **3**, ID 032006 (2021).
<https://doi.org/10.1088/2515-7639/ab97ee>.
10. Q. Peng, J. Guo, Q. Zhang, J. Xiang, B. Liu, A. Zhou, R. Liu, and Y. Tian, *J. Am. Chem. Soc.* **136**, 4113 (2014). <https://doi.org/10.1021/ja500506k>
11. M. Khazaei, M. Arai, T. Sasaki, M. Estili, and Y. Sakka, *Phys. Chem. Chem. Phys.* **17**, 7841 (2014). <https://doi.org/10.1039/C4CP00467A>
12. Y. Xie, M. Naguib, V. N. Mochalin, M. W. Barsoum, Y. Gogotsi, X. Yu, K. -W. Nam, X. -Q. Yang, A. I. Kolesnikov, and P. R. C. Kent, *J. Am. Chem. Soc.* **136**, 6385 (2014).
<https://doi.org/10.1021/ja501520b>

13. X. -H. Zha, J. Zhou, Y. Zhou, Q. Huang, J. He, J. S. Francisco, K. Luo, and S. Du, *Nanoscale* **8**, 6110 (2016). <https://doi.org/10.1039/C5NR08639F>
14. X. -H. Li, L. Shan-Shan, H. L. Cui, and R. -Z. Zhang, *ACS Omega* **5**, 22248 (2020). <https://doi.org/10.1021/acsomega.0c02435>
15. A. N. Gandi, H. N. Alshareef, and U. Schwingenschl, *Chem. Matter.* **28**, 1647 (2016). <https://doi.org/10.1021/acs.chemmater.5b04257>
16. U. Yorulmaz, A. Ozden, N. K. Perkgoz, F. Ay, and C. Sevik, *Nanotechnology* **27**, ID 335702 (2016). <https://doi.org/10.1088/0957-4484/27/33/335702>
17. S. Lai, J. Jeon, S.K. Jang, J. Xu, Y.J. Choi, J.-H. Park, E. Hwang, and S. Lee, *Nanoscale* **7**, 19390 (2015). <https://doi.org/10.1039/C5NR06513E>
18. L.-Y. Gan, D. Huang, and U. Schwingenschlogl, *J. Mater. Chem A* **1**, 13672 (2013). <https://doi.org/10.1039/C3TA12032E>
19. L. Feng, X.-H. Zha, K. Luo, Q. Huang, J. He, Y. Liu, W. Deng, and S. Du, *J. Electro. Mater.* **46**, 2460 (2017). <https://doi.org/10.1007/s11664-017-5311-5>
20. S. Rai, N. Chaurasia, and P. K. Yadawa, *Phys. Chem. Solid State* **22**, 687 (2021). <https://doi.org/10.15330/pcss.22.4.687-696>
21. D. K. Pandey, P. K. Yadawa, and R. R. Yadav, *Mater. Lett.* **61**, 5194 (2007). <https://doi.org/10.1016/j.matlet.2007.04.028>
22. W. Voigt, *Lehrbuch der kristallphysik (mitausschluss der kristalloptik)* (Leipzig Berlin, B.G. Teubner, 1966) pp. 945. <https://doi.org/10.1007/978-3-663-15884-4>
23. N. Chaurasiya, S. Rai, and P. K. Yadawa, *J. Sci. Res.* **14**, 229 (2022). <http://dx.doi.org/10.3329/jsr.v14i1.55038>
24. A. Reuss, *ZAMM – J. Appl. Math. Mechanics/Zeitschrift für Angewandte Mathematik und Mechanik* **9**, 49 (1929). <http://dx.doi.org/10.1002/zamm.19290090104>
25. R. Hill, *Proc. Phys. Soc. A* **65**, 349 (1952). <https://doi.org/10.1088/0370-1298/65/5/307>
26. N. Turkdal, E. Deligoz, H. Ozisik, and H. B. Ozisik, *Ph. Transit.* **90**, 598 (2017). <https://doi.org/10.1080/01411594.2016.1252979>
27. P. F. Weck, E. Kim, V. Tikare, and J. A. Mitchell, *Dalton Trans* **44**, 18769 (2015). <https://doi.org/10.1039/C5DT03403E>
28. D. Singh, D. K. Pandey, P. K. Yadawa, and A. K. Yadav, *Cryogenics* **49**, 12 (2009). <http://dx.doi.org/10.1016/j.cryogenics.2008.08.008>
29. V. V. Manju, S. Divakara, and R. Somashekar, *J. Sci. Res.* **12**, 607 (2020). <https://doi.org/10.3329/jsr.v12i4.47269>
30. R. R. Koireng, P. C. Agarwal, and A. Gokhroo, *J. Sci. Res.* **13**, 21 (2021). <https://doi.org/10.3329/jsr.v13i1.47327>
31. S. P. Singh, P. K. Yadawa, P. K. Dhawan, A. K. Verma, and R. R. Yadav, *Cryogenics* **100**, 105 (2019). <https://doi.org/10.1016/j.cryogenics.2019.03.006>
32. D. Singh, P. K. Yadawa, and S. K. Sahu, *Cryogenics* **50**, 476 (2010). <https://doi.org/10.1016/j.cryogenics.2010.04.005>
33. X. -H. Zha, Q. Huang, J. He, H. He, J. Zhai, J. S. Francisco, and S. Du, *Sci. Rep.* **6**, 27971 (2016). <https://doi.org/10.1038/srep27971>
34. X.-H. Zha, K. Luo, Q. Li, Q. Huang, J. He, X. Wen, and S. Du, *Europhys. Lett.* **111**, 26007 (2015). <https://doi.org/10.1209/0295-5075/111/26007>
35. N. Yadav, S. P. Singh, A. K. Maddheshiya, P. K. Yadawa, R. R. Yadav, *Phase Transitions* **93**, 883 (2020). <https://doi.org/10.1080/01411594.2020.1813290>
36. C. P. Yadav, D. K. Pandey, and D. Singh, *Indian J. Phys.* **93**, 1147 (2019). <https://doi.org/10.1007/s12648-019-01389-8>
37. A. F. Goncharov, M. Gauthier, D. Antonangeli, S. Ayrinhac, F. Decremps, M. Morand, A. Grechnev, S. M. Tretyak, and Y. A. Freiman, *Phys. Rev. B* **95**, ID 214104 (2017). <https://doi.org/10.1103/PhysRevB.95.214104>
38. P. K. Yadawa, *Adv. Mat. Lett.* **2**, 157 (2011). <https://doi.org/10.5185/amlett.2010.12190>
39. J. Feng, B. Xiao, C. L. Wan, Z. X. Qu, Z. C. Huang, J. C. Chen, R. Zhou, and W. Pan, *Acta Mater.* **59**, 1742 (2011). <https://doi.org/10.1016/j.actamat.2010.11.041>

40. A. K. Jaiswal, P. K. Yadawa, and R. R. Yadav, *Ultrasonics* **89**, 22 (2018). <https://doi.org/10.1016/j.ultras.2018.04.009>
41. S. P. Singh, G. Singh, A. K. Verma, P. K. Yadawa, and R. R. Yadav, *Pramana-J. Phys.* **93**, 83 (2019). <https://doi.org/10.1007/s12043-019-1846-8>
42. P. K. Yadawa, *Ceramics-Silikaty* **55**, 127 (2011). <https://doi.org/10.12691/jmpc-3-1-1>
43. P. K. Yadawa, *Arab. J. Sci. Eng.* **37**, 255 (2012). <https://doi.org/10.1007/s13369-011-0153-6>